AGU ADVANCING EARTH AND SPACE SCIENCE

Geophysical Research Letters®

RESEARCH LETTER
10.1029/2021GL095302

Key Points:

- A deep-learning approach termed FURENet is proposed for convective precipitation nowcasting with multiple input variables
- Polarimetric radar variables are used to provide microphysics and dynamic structure information of convective storms in the model
- Experiments with FURENet show significant improvement on nowcasting performance

Supporting Information:

Supporting Information may be found in the online version of this article.

Correspondence to:

K. Zhao,
zhaokun@nju.edu.cn

Citation:

Pan, X., Lu, Y., Zhao, K., Huang, H., Wang, M., & Chen, H. (2021). Improving nowcasting of convective development by incorporating polarimetric radar variables into a deep-learning model. *Geophysical Research Letters*, *48*, e2021GL095302. https://doi.org/10.1029/2021GL095302

Received 16 JUL 2021
Accepted 13 OCT 2021

Improving Nowcasting of Convective Development by Incorporating Polarimetric Radar Variables Into a Deep-Learning Model

Xiang Pan[1,2], Yinghui Lu[1,2], Kun Zhao[1,2], Hao Huang[1,2], Mingjun Wang[3], and Haonan Chen[4,5]

[1]Key Laboratory of Mesoscale Severe Weather/MOE and School of Atmospheric Sciences, Nanjing University, Nanjing, China, [2]State Key Laboratory of Severe Weather and Joint Center for Atmospheric Radar Research of CMA/NJU, Beijing, China, [3]Nanjing Joint Institute for Atmospheric Sciences, Nanjing, China, [4]Department of Electrical and Computer Engineering, Colorado State University, Fort Collins, CO, USA, [5]NOAA Physical Sciences Laboratory, Boulder, CO, USA

Abstract Nowcasting of convective storms is urgently needed yet rather challenging. Current nowcasting methods are mostly based on radar echo extrapolation, which suffer from the insufficiency of input information and ineffectiveness of model architecture. A novel deep-learning (DL) model, FURENet, is designed for extracting information from multiple input variables to make predictions. Polarimetric radar variables, K_{DP} and Z_{DR}, which provide extra microphysics and dynamic structure information of storms, are fed into the model to improve nowcasting. Two representative cases indicate that K_{DP} and Z_{DR} can help the DL model better forecast convective organization and initiation. Quantitative statistical evaluation shows using FURENet, K_{DP}, and Z_{DR} synergistically improve nowcasting skills (CSI score) by 13.2% and 17.4% for the lead time of 30 and 60 min, respectively. Further evaluation shows the microphysical information provided by the polarimetric variables can enhance the DL model in understanding the evolution of convective storms and making more trustable nowcasts.

Plain Language Summary Severe convective precipitation is a major cause of many hazards. However, very short-term forecasting, i.e., nowcasting, of convective precipitation is rather challenging. Current nowcasting methods suffer from insufficiency of physics information of input data and ineffectiveness of model architecture. As an advanced observing tool, polarimetric weather radar can provide crucial microphysics and dynamic structure information of convective precipitation systems. To incorporate polarimetric radar variables into the nowcasting task, this study proposes a novel model architecture termed FURENet based on deep learning. FURENet uses U-Net as a flexible backbone, and is specially designed to facilitate exploiting information from multiple input variables. By training the model with polarimetric radar variables (K_{DP} and Z_{DR}) as input, significant improvement of forecasting the initiation, development and evolution of convective storms is achieved. The results also show the effectiveness of model architecture.

1. Introduction

Severe convective precipitation is a major cause of many hazards such as floods and mudslides that lead to massive economic losses and casualties. Unfortunately, the characteristics such as rapid development, short life cycle and highly nonlinear dynamics of convective precipitation make it rather challenging to be precisely forecasted. Very short-term forecasting, that is, nowcasting, of convective precipitation using weather radar observations, has raised extensive research interest. Wilson et al. (1998) made a comprehensive review of convective storm characteristics and nowcasting methods, and pointed out that the insufficiency of data information and the ineffectiveness of nowcasting model are the two major challenges that convective precipitation nowcasting faces. Although improved over the past decades, these two deficiencies still remain to be settled (Ayzel et al., 2019; Chen et al., 2020; Sun et al., 2014; Wilson et al., 2010).

Traditional nowcasting methods are mostly based on extrapolation of radar echo maps or satellite images, either by first identifying storms then tracking and extrapolating them (del Moral et al., 2018; Dixon & Wiener, 1993; Gagne et al., 2017; Li et al., 1995), or by estimating the flow field (Ayzel et al., 2019; Lucas &

Kanade, 1981). Despite of the capability to predict very short-term linear advection characteristics of the storms, these extrapolation-based methods can hardly forecast initiation and evolution of convective storms especially when the lead time is longer than 30 min (Gultepe et al., 2019; Wilson et al., 1998). Recently, as a strong tool of automatically extracting information from massive data and making prediction, deep-learning (DL)-based methods (Lecun et al., 2015) have drawn great attention in geophysical studies such as rainfall estimation (Chen et al., 2019), gravity wave parameterization (Matsuoka et al., 2020), and ENSO prediction (Petersik & Dijkstra, 2020). There are also attempts to leverage deep learning in precipitation nowcasting (Chen et al., 2019; Shi et al., 2015; Sønderby et al., 2020). However, these studies suffer from the lack of physical process information within input data (mostly only radar reflectivity or satellite images), thus are still limited in making precise nowcasting of convective storms (Han et al., 2019; Zhou et al., 2020). Moreover, to extract information from multiple input variables, the model architecture should have more specialized design (Baltrušaitis et al., 2018).

From the perspective of input data, polarimetric radar variables such as Z_{DR} and K_{DP} can provide richer information of microphysics in convective storms than radar reflectivity (Doviak & Zrnic, 1993; Kumjian, 2013; Zhao et al., 2019). The differential reflectivity Z_{DR} (Seliga & Bringi, 1976, 1978) is the logarithmic difference between the horizontally and vertically polarized waves and is therefore positive for large rain drops (typically with oblate shapes), and close to zero for hails (typically with nearly spherical shapes, Brandes et al., 2002; Thurai et al., 2009). The specific differential phase K_{DP} is the derivative with respect to radar range of differential phase (Φ_{DP}) from two polarized waves, and K_{DP} is closely related to the liquid water content in different areas of storms (Zrnić & Ryzhkov, 1996). In addition, recent studies have shown the spatial patterns of polarimetric radar variables have the potential of revealing structure and evolution information about storms, which are promisingly beneficial for convective nowcasting. For instance, high value of arc-shaped Z_{DR} appeared at middle or low level usually indicates large vertical wind shear (Kumjian & Ryzhkov, 2008) or strong storm-relative wind profile (Dawson et al., 2015). The signs of Z_{DR} column (Kumjian, 2013) and K_{DP} foot (Romine et al., 2008) also conveys the dynamical information of strong updraft and low-level convergent boundary. The patterns of Z_{DR}, K_{DP}, and reflectivity reveal distinct characteristics of size and distribution of raindrops, which may change dramatically during different evolution stages of storms and thus provide evolution information about storms (Wang et al., 2016; Wen et al., 2017). Therefore, polarimetric radar variables have a great potential to improve nowcasting of convective precipitation.

From the perspective of models, Shi et al. (2015) proposed Convolutional Long Short-Term Memory (ConvLSTM), a spatiotemporal-forecasting neural network model, as a first attempt for DL-based precipitation nowcasting. This work is then followed by a number of studies (Shi et al., 2017; Sønderby et al., 2020; Wang et al., 2017). However, since the structure of ConvLSTM is relatively fixed, current ConvLSTM-based nowcasting methods hardly have specially designed structure for multiple input information. Another effective DL architecture in computer vision filed is U-Net (Ronneberger et al., 2015), which is based on multilayer convolutional neural networks and used by various image-to-image translation tasks. Compared with the ConvLSTM-based models, the U-Net has more flexible architecture, which can be easily adjusted for exploiting multiple input information. The U-Net is increasingly used by spatiotemporal forecasting studies, such as nowcasting of lightnings (Zhou et al., 2020) and global weather forecasting (Weyn et al., 2020). As such, we choose U-Net as our backbone model in this study.

Moreover, utilizing multiple information in DL, also known as *multimodal learning*, is drawing growing interests (Baltrušaitis et al., 2018). A typical way of multimodal learning is to concatenate multiple variables at the "channel" dimension of the very first layer of convolutional networks (Han et al., 2019; Jing et al., 2019). However, such concatenation, also known as *early-fusion*, tends to suffer from the information entanglement effect, which undermines the performance of the model (Baltrušaitis et al., 2018; Dolz et al., 2018). In contrast, several studies have proved that the combination of multiple variables in deeper layer, i.e., *late-fusion* strategy, helps the model learn each individual modality better and also allow for more flexibility (Tseng et al., 2017; Zhou et al., 2019). In addition, DL-based video processing studies show that *attention mechanisms* can be leveraged to help better handle multimodal input data (Fan et al., 2019; Long et al., 2018). As types of observation available for nowcasting grow rapidly, DL-based nowcasting task should also consider the issue of multimodal learning. It is worth noting that such multimodal DL-based

approaches are also urgently needed in general geophysical research, since the surging amounts of observation are also generally characteristic of geophysical researches (Reichstein et al., 2019).

Therefore, this study aims to design a deep learning architecture to facilitate exploiting multiple input information, and effectively leverage microphysics and dynamic structure information of polarimetric radar variables, to make more precise and physics-consistent nowcasting of convective precipitation. The model we established is named as Fusion and Reassignment Networks (FURENet).

2. Data Set and Experimental Design

2.1. NJU-CPOL Data Set

This study uses data from a C-band dual polarization weather radar operated by Nanjing University. The data set (termed NJU-CPOL) is collected during 2014–2019, covering 268 precipitation events. The raw radar data are first quality-controlled (Huang et al., 2018) and then interpolated to the Cartesian coordinate, with the spatial resolution of 1 km in horizontal. In this study, we use the data of 3 km altitude CAPPI (Constant Altitude Plan Projection Indicator) with 256 × 256 km area around the radar center. The temporal resolution of the data set is 6–7 min.

2.2. Experimental Design

As illustrated in Equation 1, the nowcasting problem is defined as using 1-h radar reflectivity (Z_H) and optional polarimetric variables (K_{DP} and Z_{DR}) before the present time, to predict reflectivity in the next 1 h. Observations at different time steps are stacked together to form the *channel* dimension

$$\hat{Z}_{H;t+1},\ldots,\hat{Z}_{H;t+K} = \mathcal{M}\left(\begin{array}{l} Z_{H;t-J+1},\ldots,Z_{H;t};\\ \left(\text{Optional}\right)Z_{\mathrm{DR};t-j+1,\ldots},Z_{\mathrm{DR};t}\left(\text{Optional}\right)K_{\mathrm{DP};t-j+1,\ldots},K_{\mathrm{DP};t}\end{array}\right), \tag{1}$$

where $\mathcal{M}$ is the nowcasting model, J and K are time steps of input and output and both equal to 10 as the time interval of radar observation is 6–7 min. As such, a single *sample* contains radar data of 20 time steps in total. After filtering out nonrainy days (see in Supporting Information S1), 10,672 samples remain in the data set. We set samples collected after September 2019 as independent testing data set (1,056 samples) and the rest as the training data set (9,616 samples), making the train-test splitting ratio roughly 9:1, as a general machine learning setting.

Three experiments Zh_FURE, ZhKdp_FURE, and ZhKdpZdr_FURE, using FURENet architecture, are designed to examine the impact of including polarimetric radar variables into the model. The experiment Zh_FURE uses only radar reflectivity as input, while ZhKdp_FURE adds only K_{DP} and ZhKdpZdr_FURE adds K_{DP} and Z_{DR} together as input. We also perform two baseline experiments Zh_OF (using "Dense" optical flow method in Ayzel et al., 2019) and Zh_TGRU (using TrajGRU, Shi et al., 2017, as a benchmark DL model) to evaluate the performance of the FURENet model compared to other nowcasting methods. To further evaluate the improvement made by specially designed architecture, we also include an experiment ZhKdpZdr_U using the same input variables as ZhKdpZdr_FURE, but without *late-fusion* strategy or *SE-block* (see in Section 3).

3. Methodology

3.1. U-Net

The main pipeline and schematic illustration of our model architecture are shown in Figure 1. The U-Net is used as the backbone model since it has more flexible architecture and lower computational cost compared to explicit recurrent network architectures (i.e., ConvLSTM-based models). The architecture comprises two basic parts: an encoder and a decoder. The encoder extracts spatiotemporal information from input data by down-sampling the frames with convolution operations. Then the extracted spatiotemporal information is passed to the decoder, which makes prediction by up-sampling the features. As illustrated by the purple lines, the intermediate state tensors (colored cubes) of the encoder are concatenated to the tensors at the

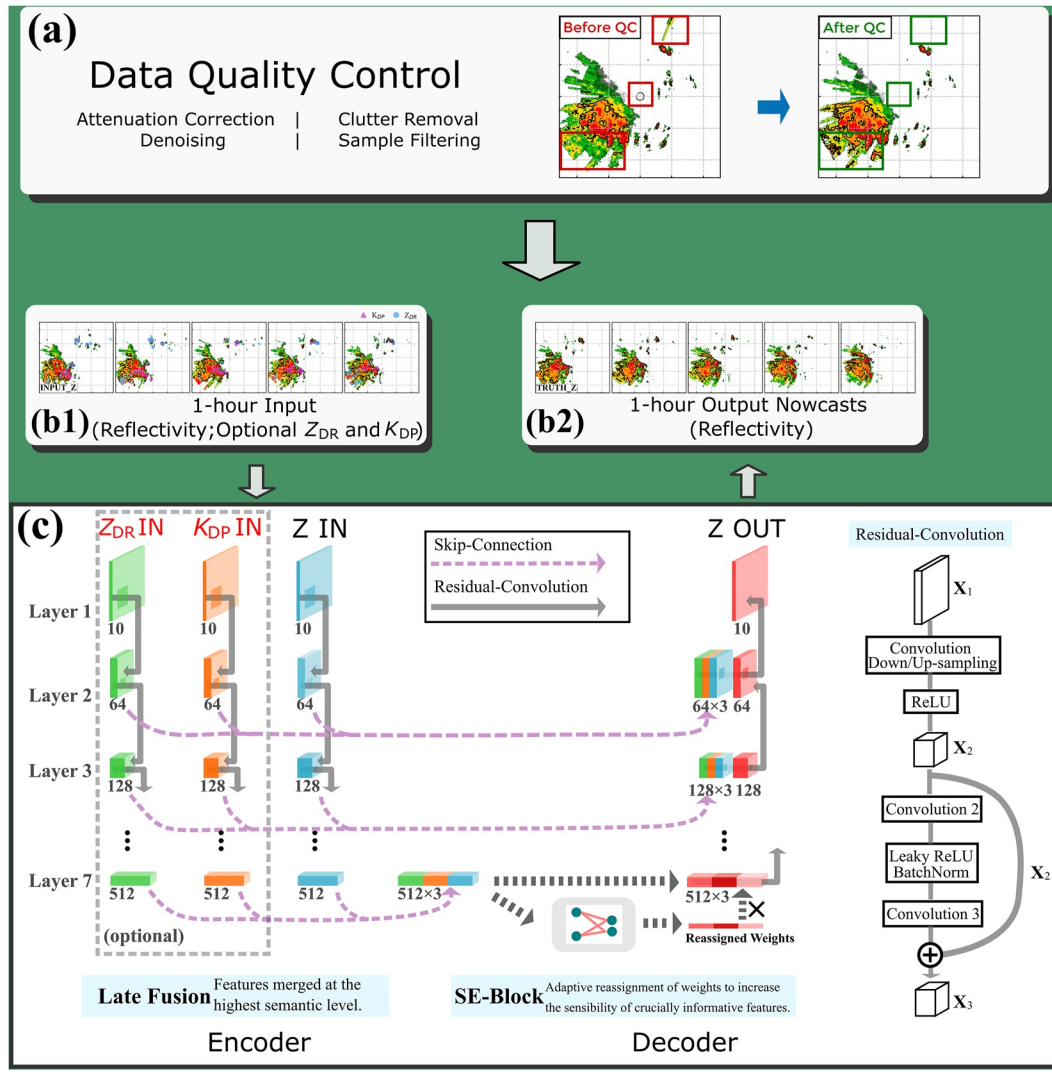

Figure 1. Main pipeline and schematic illustration of FURENet architecture. The feature numbers at each layer are noted in gray. (a) The polarimetric radar data are passed through a standard quality control procedure first. (b) Then 1-h data before the present time is fed into the model. (c) Multiple polarimetric radar variables are encoded with different branches of the encoder and merged at the highest semantic level, namely *late-fusion*. Then the weights of the features are adaptively reassigned by the *SE-block* and then passed to the decoder to make the final prediction.

same level of the decoder. Such concatenation, also known as "skip-connection," empowers the model to maintain multiscale spatial information in the input data, thus capable of capturing the evolution characteristics of various precipitation systems. In addition, we add extra convolutional operations with residual connections in each layer of the U-Net model (as shown in Figure 1c), since the residual connections lead to easier optimization and higher representative capability for deeper networks (He et al., 2016).

3.2. Late-Fusion Strategy

A typical way to utilize multiple input variables in deep-learning models is to concatenate the variable fields at the "channel" dimension as the input of the first convolutional layer (Weyn et al., 2020; Zhou et al., 2020). This concatenation, also known as *early-fusion*, has an underlying assumption that the input variables are at the same semantic level thus can be linearly combined to pass through the next layer (Baltrušaitis et al., 2018). However, the assumption may not hold when there exist more complex dependencies in the input variables, incurring possible information entanglement effects. To address this problem, we apply the

late-fusion strategy in the encoder, where the different variables are first encoded independently, and then combined at their highest semantic level (as shown in Figure 1c). In this way, the model is empowered to learn more complex dependencies between multiple information (Pandeya & Lee., 2021; Tseng et al., 2017; Zhou et al., 2019). To the best of our knowledge, this is the first study to apply the late-fusion strategy in meteorology forecasting problems.

3.3. Adaptive Importance Reassignment

As there exist inherent deficiencies of radar operating principles and data preprocessing algorithms, the data fed into the model can sometimes have noise or unexpected biases. In a specific nowcasting case, when multiple variables are encoded together as a high-level representation (the bottommost cubes in Figure 1c), the variables with low quality may reduce the final prediction precision. To solve this problem, the model must possess the capability of adaptively reassigning the importance of multiple variables, i.e., to lower the weights of features undermining the prediction and raise the weights of features benefitting the prediction. In this study, we achieve this goal by inserting a "squeeze and excitation block" (SE-block) after the late-fusion of multiple variables. This technique, also known as *channel-wise attention*, helps the model adaptively learn to reassign the importance of variable features (Hu et al., 2018).

As in Figure 1c, the high-level representative tensors are first passed through a global pooling "squeeze" operation, where the tensors are averaged over their spatial dimensions (*Height* × *Width*), reduced to a vector of global channel features. Then an "excitation" operation, which is a 2-layer fully connected bottleneck multilayer perceptron neural network and operates as an adaptively self-gating mechanism, is applied to obtain the vector of learned weights. The weights have the same length of the number of features in high-level tensors, representing the reassigned importance of the original features. Finally, these learned weights are multiplied back to the high-level tensors to get a final importance-reassigned tensor. Such an explicit weight reassignment mechanism can also be interpreted as disentanglement of spatial and feature-wise information, enabling the model to increase the sensibility of crucially informative features thus benefit the forecasting.

3.4. FURENet

In short, the overall FURENet architecture comprises an encoder with multiple branches to achieve the late-fusion strategy, followed by an SE-block at the highest semantic level, and a decoder. Both encoder and decoder have seven main layers, in which tensors are continuously calculated by grouped residual-convolution operation. Detailed settings of the hyperparameters and the training procedure are shown in Table S1.

4. Results

4.1. Representative Cases

Two representative cases in the testing data set that illustrate how the polarimetric radar variables benefit the nowcasting are presented in Figures 2 and 3.

Figure 2 shows the input (a1–a5, reflectivity including optional polarimetric variables), evaluation truth (b1–b5, reflectivity), and outputs from five experiments Zh_OF, Zh_TGRU, Zh_FURE, ZhKdp_FURE, and ZhKdpZdr_FURE (c1–g5, reflectivity), of a convective organization case happened at 19:13 to 21:31 UTC, on September 15, 2019, Guangdong. For conciseness, we display radar maps every two frames. As observed in the input sequence (Figures 2a1–2a5), the Area B is characterized by linearly distributed large Z_{DR} and moderate K_{DP} values (Figures 2a3–2a5), which indicate large drops with relatively low concentration in the early evolution stage of the convective system (Wen et al., 2017). However, the pattern of reflectivity in Area B is of unobvious size (diameter <5 km) even at the last input frame (Figure 2a5), which fails to provide a clear convective organizing signal to DL-based models. In the afterward evaluation truth (Figure 2b1–2b5), the storm in Area B gradually organized, and developed into a linear convective system. In Zh_OF, optical flow fails to forecast this evolution. Using only reflectivity as input, the forecasted storms in Zh_TGRU and

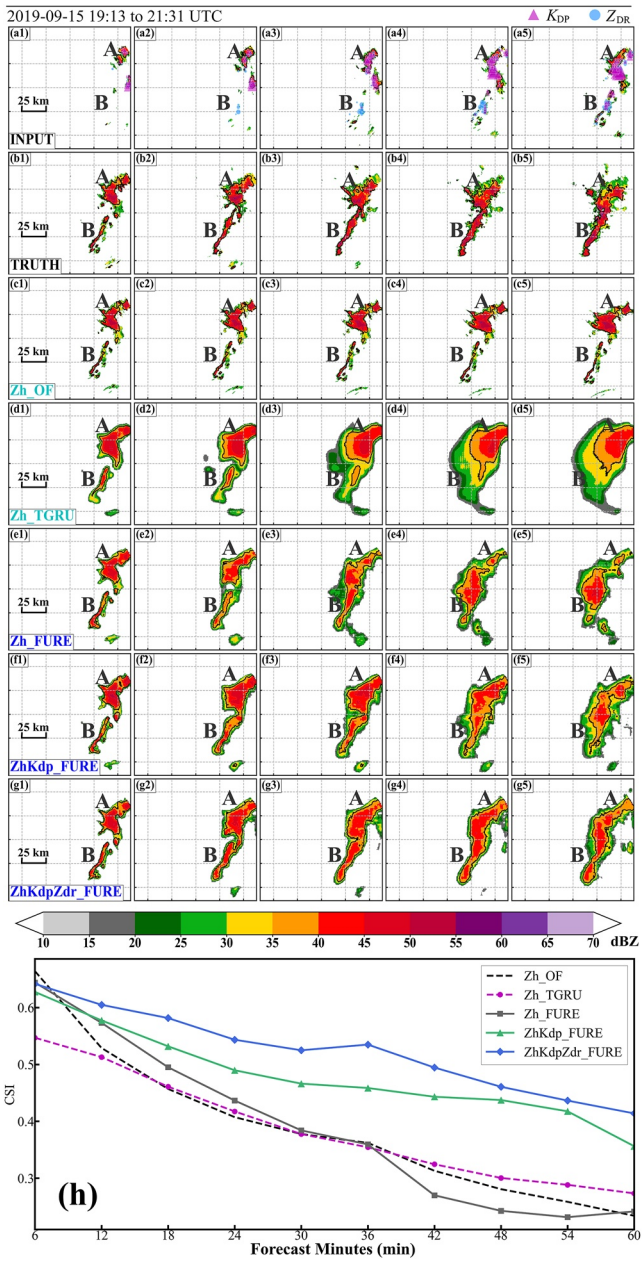

Figure 2. A representative case of convective organization (in Area B). Reflectivity (and Z_{DR}, K_{DP}) observations of inputs (a1–a5) and afterward ground truth (b1–b5) and nowcasts from experiment Zh_OF (c1–c5), Zh_TGRU (d1–d5), Zh_FURE (e1–e5), ZhKdp_FURE (f1–f5), and ZhKdpZdr_FURE (g1–g5) corresponding to 12-min (first column), 24-min (second column), 36-min (third column), 48-min (fourth column), and 60-min (fifth column) forecasts. For conciseness, K_{DP} (Z_{DR}) with values larger than 1 deg km^{-1} (1 dB) is plotted with purple triangles (blue circles), whose sizes indicate the value of K_{DP} (Z_{DR}). (h) CSI time series for 35 dBZ threshold. Detailed contours of K_{DP}/Z_{DR} can be found in the Supporting Information S1.

Zh_FURE (Figure 2d1–2d5 and 2e1–2e5), are with inaccurate shape and intensity. However, as the pattern of Z_{DR} and K_{DP} clearly depicts a linear system, the experiments ZhKdp_FURE and ZhKdpZdr_FURE (Figure 2f1–2f5 and 2g1–2g5) both capture this useful signal and make successful forecasts of this linear organization process. In addition, the storm in Area A is better forecasted with added polarimetric variables, both in aspects of spatial extent and intensity distribution. The CSI (critical success index) score defined as hits/(hits + misses + false alarms), where 35 dBZ threshold is used to identify strong convections (Dixon & Wiener, 1993), is utilized to quantitatively evaluate nowcast performance. As shown in Figure 2h, ZhKdp_FURE and ZhKdpZdr_FURE continuously outperform other methods.

Another convective initiation case (shown in Figure 3) happened during 05:58 to 08:16 UTC, October 07, 2019 also indicates the benefits that polarimetric radar variables offer to the nowcasting model. In the Area A of input sequence (Figure 3a1–3a5), large K_{DP} and Z_{DR} values are observed. As shown in the afterward observation sequence (Figure 3b1–3b5), a new convective cell initiates in Area A. Nowcasts of Zh_OF (Figure 3c1–3c5) fail to predict the movement in Area B and the convective initiation in Area A. The forecasts in Zh_TGRU and Zh_FURE (Figure 3d1–3d5 and 3e1–3e5) also fail to predict this convective initiation process because the irregular pattern of reflectivity shows scarce sign about that, while the experiments ZhKdp_FURE and ZhKdpZdr_FURE, which include polarimetric variables (Figure 3f1–3f5 and 3g1–3g5), both make accurate forecasts about the storm initiated in Area A. In addition, the storm in Area B is also forecasted more precisely by the ZhKdp_FURE and ZhKdpZdr_FURE, both in spatial extent and intensity distribution. The quantitative evaluation (Figure 3h) also demonstrates the superiority of ZhKdp_FURE and ZhKdpZdr_FURE.

The nowcasting results on the two representative cases indicate that polarimetric variables included in FURENet offer an opportunity to better forecast initiation and organization of convective storms, which are major concerns in convective nowcasting tasks. It is noted that the current nowcasting model shares the common weakness with other DL-based nowcasting models that the forecasted patterns of reflectivity are sometimes blurred (Tran & Song, 2019; Veillette et al., 2020). One example of such poor nowcast due to blur effect is given in Figure S3. However, the overall quantitative performance is significantly improved by including polarimetric variables into the FURENet, which is introduced in Section 4.2.

4.2. Quantitative Performance Evaluation

The overall nowcasting performance on the testing data set is quantitatively evaluated with CSI for 35 dBZ threshold. It is noted that owing to unavoidable difference of implementation, data sets and evaluation metrics, the scores of baseline models in this study may be somehow different from original studies. As shown in Figure 4a, all deep-learning based models outperform optical flow nowcasting algorithm (Zh_OF). When using reflectivity as the only predictor, FURENet (Zh_FURE) performs slightly better than recurrent-structured neural networks (Zh_TGRU). Using FURENet architecture, experiment ZhKdp_FURE shows relative improvements of 4.4% and 13.3% in 30-min and 60-min nowcasts over experiment Zh_FURE. Experiment ZhKdpZdr_FURE reaches even higher performance with 13.2% and 17.4% relative improvements over experiment Zh_FURE in 30-min

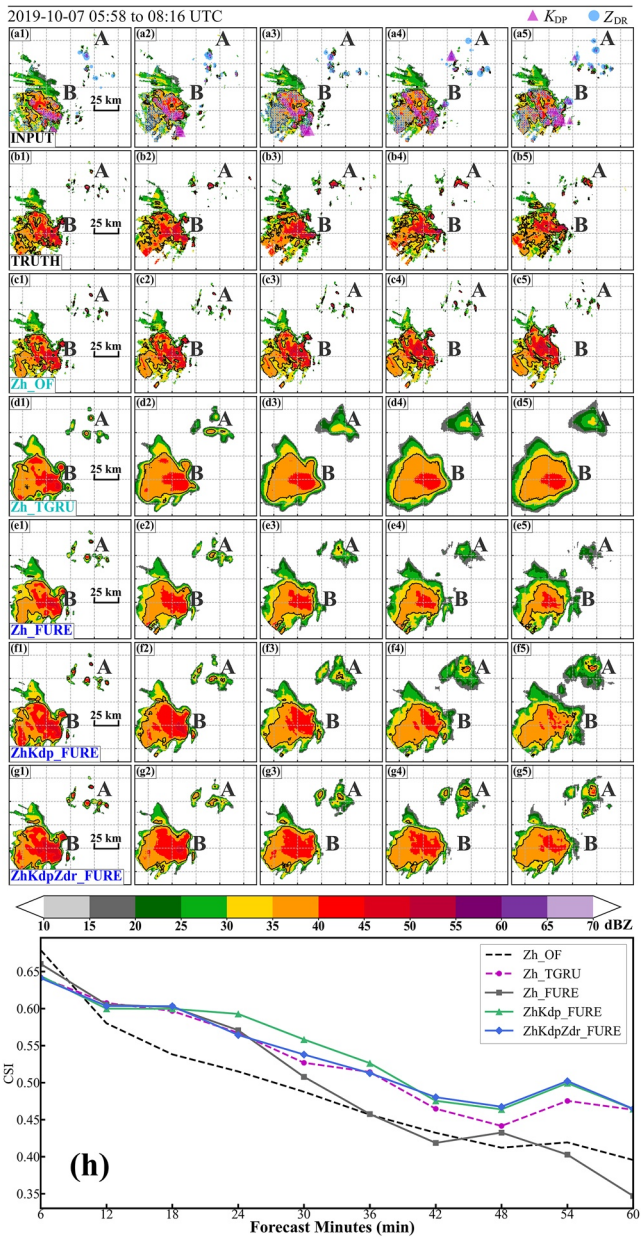

Figure 3. Same as Figure 2. But for a representative case of convective initiation (in Area A).

and 60-min nowcasts. The experiment ZhKdpZdr_U uses the same input variables as ZhKdpZdr_FURE, but with neither *late-fusion* strategy nor *SE-block*. Clear superiority of the FURENet architecture (9.0% and 14.8% improvement on 30-min and 60-min nowcasts, respectively) on exploiting information from multimodal polarimetric radar data is observed. The results indicate that microphysics information in polarimetric radar variables and the effectiveness of the FURENet architecture to utilize the extra information successfully improve the forecasting skill, especially in the longer forecasting period.

The nowcasting scores as a function of lead time are illustrated in Figure 4b. As illustrated, the scores of Zh_TGRU and Zh_FURE descends rapidly with time. However, ZhKdp_FURE and ZhKdpZdr_FURE show a clear superiority to Zh_FURE and Zh_TGRU, because K_{DP} and Z_{DR} can provide richer information about microphysics and dynamical structures, which improves the forecast of initiation and irregular evolution of convective storms at longer lead time.

In addition, forecasting skill with different convective area variation rate (CAVR) is also evaluated (Figure 4c). CAVR represents simple but robust characteristic of convective system evolution, and is defined as

$$\mathrm{CAVR} = \frac{1}{\mathrm{NS}} \sum_{t=0}^{T-30\mathrm{min}} \left(C_{t+30\mathrm{min}} - C_t \right) \times 1000 \qquad (2)$$

where C_t is the total area above the threshold of 35 dBZ, T is the time span of foresting period, N is the number of $\left(C_{t+30\mathrm{min}} - C_t \right)$ pairs, and S is the area of the whole observation field. As such, positive (negative) CAVR values mean the increase (decrease) of convective area, which indicates the convective system is developing (dissipating). As shown in Figure 4b, ZhKdp_FURE and ZhKdpZdr_FURE both outperform Zh_FURE among all samples of different CAVRs. Moreover, among the samples with negative CAVRs, ZhKdpZdr_FURE gains higher increments of scores over ZhKdp_FURE and Zh_FURE, while the scores of ZhKdp_FURE and ZhKdpZdr_FURE get closer among the samples with positive CAVRs. These results indicate the pattern of Z_{DR} provides the DL models with crucial information of convective storms in maturer or dissipative stages, and the pattern of K_{DP} leads to better forecasts of convective development processes. Both of the polarimetric variables synergistically help the DL model better understand the characteristics of convective storms evolution thus making more trustable nowcasts. Quantitative evaluation for the reflectivity threshold of 15 dBZ is also performed, as shown in Figure S4.

5. Summary and Discussion

A novel deep-learning model FURENet for convective precipitation nowcasting is proposed and demonstrated with multiple polarimetric radar variables as input. The model uses the U-Net model as backbone and is specially designed to facilitate exploiting information from multiple input variables to make the prediction. Two-specialized design, i.e., late-fusion and SE-block, assists the model to better capture and manage multimodal information thus benefit the forecasting. A new data set NJU-CPOL containing multiple dual polarimetric radar variables of precipitation events in 2014–2019 is presented for precipitation nowcasting task. Two polarimetric radar variables, K_{DP} and Z_{DR}, are used to provide crucial microphysics and dynamic evolution information of convective storms, which benefit DL-based nowcasting. Two representative nowcasting cases show that polarimetric variables offer an opportunity for deep-learning model to better forecast the organization and

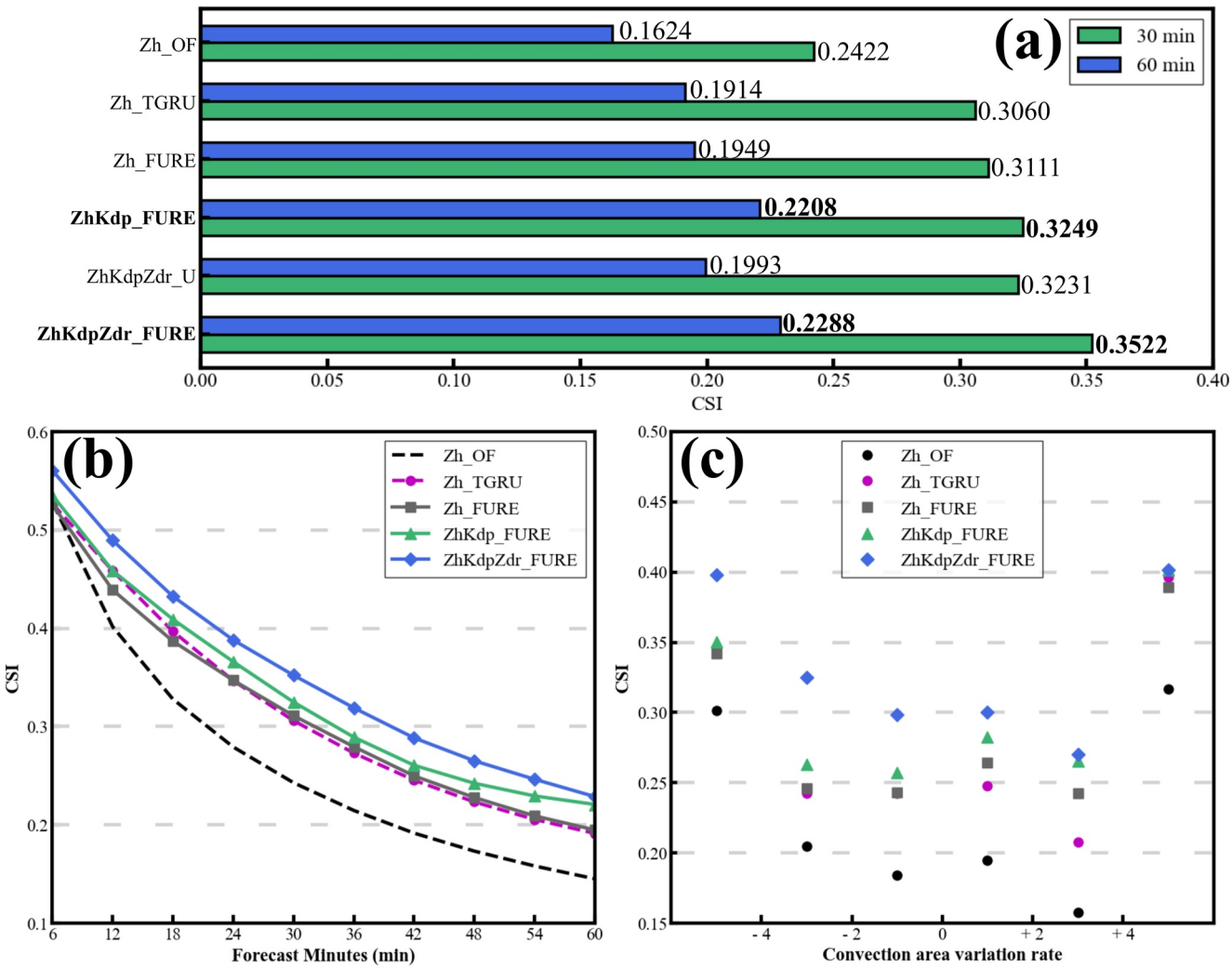

Figure 4. (a) Critical success index (CSI) for 35 dBZ threshold of 30-min (green) and 60-min (blue) nowcasts from different experiments, (b) CSI of 60-min nowcasts, and (c) CSI for 35 dBZ threshold versus convection area variation rate, from experiment Zh_OF (black), Zh_TGRU (magenta), Zh_FURE (gray), ZhKdp_FURE (green), and ZhKdpZdr_FURE (blue).

initiation of convective storms. Quantitative evaluation further shows that K_{DP} and Z_{DR} synergistically and significantly improve the nowcasting skill at longer forecasting period and provide better forecasts of convective development processes. These results indicate that leveraging appropriate deep-learning models to exploit the underlying physics in polarimetric radar variables leads to more precise and physics-consistent forecasts, and thus has great potential to release the long-standing challenge of nowcasting the initiation and irregular evolution of convective storms in longer nowcasting period.

The architecture presented here is GPU memory efficient (see in Table S2), so that the model is welcome for extensive input features. The model is not task specific only for precipitation nowcasting. Various field-to-field forecasting or transformation tasks, such as climate predicting and hydrometeor classification can choose this model as a reliable baseline as long as there exists multiple field variables to provide information. The current study focuses on the two-dimensional CAPPI polarimetric radar observations. However, three-dimensional polarimetric radar observations as well as numerical model variables would have more comprehensive structural information about convective storms and useful environmental features. The tests of adding these additional features into the model to improve nowcasting will be carried out in future study. Further improvements on model architecture that can facilitate fusion of multiple variable information will also be investigated in the future.

Data Availability Statement

The NJU-CPOL data set are available at https://doi.org/10.5281/zenodo.5109403.

Acknowledgments
This work was primarily supported by the National Natural Science Foundation of China (Grants 42025501, 41875053, 41805025, 41875054, and 61827901), the National Key Research and Development Program of China (Grant 2017YFC1501703), as well as the Open Research Program of the State Key Laboratory of Severe Weather.

References

Ayzel, G., Heistermann, M., & Winterrath, T. (2019). Optical flow models as an open benchmark for radar-based precipitation nowcasting (rainy motion v0. 1). *Geoscientific Model Development*, *12*(4), 1387–1402. https://doi.org/10.5194/gmd-12-1387-2019

Baltrušaitis, T., Ahuja, C., & Morency, L. P. (2018). Multimodal machine learning: A survey and taxonomy. *IEEE Transactions on Pattern Analysis and Machine Intelligence*, *41*(2), 423–443. https://doi.org/10.1109/TPAMI.2018.2798607

Brandes, E. A., Zhang, G., & Vivekanandan, J. (2002). Experiments in rainfall estimation with a polarimetric radar in a subtropical environment. *Journal of Applied Meteorology*, *41*(6), 674–685. https://doi.org/10.1175/1520-0450(2002)041<0674:EIREWA>2.0.CO;2

Chen, H., Chandrasekar, V., Tan, H., & Cifelli, R. (2019). Rainfall estimation from ground radar and TRMM precipitation radar using hybrid deep neural networks. *Geophysical Research Letters*, *46*, 10669–10678. https://doi.org/10.1029/2019GL084771

Chen, L., Cao, Y., Ma, L., & Zhang, J. (2020). A deep learning-based methodology for precipitation nowcasting with radar. *Earth and Space Science*, *7*, e2019EA000812. https://doi.org/10.1029/2019EA000812

Dawson, D. T., Mansell, E. R., & Kumjian, M. R. (2015). Does wind shear cause hydrometeor size sorting? *Journal of the Atmospheric Sciences*, *72*(1), 340–348. https://doi.org/10.1175/JAS-D-14-0084.1

del Moral, A., Rigo, T., & Llasat, M. C. (2018). A radar-based centroid tracking algorithm for severe weather surveillance: Identifying split/merge processes in convective systems. *Atmospheric Research*, *213*, 110–120. https://doi.org/10.1016/j.atmosres.2018.05.030

Dixon, M., & Wiener, G. (1993). TITAN: Thunderstorm Identification, Tracking, Analysis, and Nowcasting—A radar-based methodology. *Journal of Atmospheric and Oceanic Technology*, *10*(6), 785–797. https://doi.org/10.1175/1520-0426(1993)010<0785:TTITAA>2.0.CO;2

Dolz, J., Ayed, I. B., & Desrosiers, C. (2018). Dense multi-path U-Net for ischemic stroke lesion segmentation in multiple image modalities. In *International MICCAI Brainlesion Workshop* (pp. 271–282). Springer. https://doi.org/10.1007/978-3-030-11723-8_27

Doviak, R. J., & Zrnic, D. S. (1993). *Doppler radar and weather observations*. Courier Corporation. https://doi.org/10.1016/C2009-0-22358-0

Fan, C., Zhang, X., Zhang, S., & Huang, H. (2019). Heterogeneous memory enhanced multimodal attention model for video question answering. In *Proceedings of the IEEE/CVF Conference on Computer Vision and Pattern Recognition* (pp. 1999–2007).

Gagne, D. J., McGovern, II, A., Haupt, S. E., Sobash, R. A., Williams, J. K., & Xue, M. (2017). Storm-based probabilistic hail forecasting with machine learning applied to convection-allowing ensembles. *Weather and Forecasting*, *32*(5), 1819–1840. https://doi.org/10.1175/WAF-D-17-0010.1

Gultepe, I., Sharman, R., Williams, P. D., Zhou, B., Ellrod, G., Minnis, P., et al. (2019). A review of high impact weather for aviation meteorology. *Pure and Applied Geophysics*, *176*(5), 1869–1921. https://doi.org/10.1007/s00024-019-02168-6

Han, L., Sun, J., & Zhang, W. (2019). Convolutional neural network for convective storm nowcasting using 3-D doppler weather radar data. *IEEE Transactions on Geoscience and Remote Sensing*, *58*(2), 1487–1495. https://doi.org/10.1109/TGRS.2019.2948070

He, K., Zhang, X., Ren, S., & Sun, J. (2016). Deep residual learning for image recognition. In *Proceedings of the IEEE Conference on Computer Vision and Pattern Recognition* (pp. 770–778).

Hu, J., Shen, L., & Sun, G. (2018). Squeeze-and-excitation networks. In *Proceedings of the IEEE Conference on Computer Vision and Pattern Recognition* (pp. 7132–7141). https://doi.org/10.1109/cvpr.2018.00745

Huang, H., Zhao, K., Zhang, G., Lin, Q., Wen, L., Chen, G., et al. (2018). Quantitative precipitation estimation with operational polarimetric radar measurements in Southern China: A differential phase-based variational approach. *Journal of Atmospheric and Oceanic Technology*, *35*(6), 1253–1271. https://doi.org/10.1175/JTECH-D-17-0142.1

Jing, J., Li, Q., & Peng, X. (2019). MLC-LSTM: Exploiting the spatiotemporal correlation between multi-level weather radar echoes for echo sequence extrapolation. *Sensors*, *19*(18), 3988. https://doi.org/10.3390/s19183988

Kumjian, M. R. (2013). Principles and applications of dual-polarization weather radar. Part I: Description of the polarimetric radar variables. *Journal of Operational Meteorology*, *1*(19), 226–242. https://doi.org/10.15191/nwajom.2013.0119

Kumjian, M. R., & Ryzhkov, A. V. (2008). Polarimetric signatures in supercell thunderstorms. *Journal of Applied Meteorology and Climatology*, *47*(7), 1940–1961. https://doi.org/10.1175/2007JAMC1874.1

LeCun, Y., Bengio, Y., & Hinton, G. (2015). Deep learning. *Nature*, *521*(7553), 436–444. https://doi.org/10.1038/nature14539

Li, L., Schmid, W., & Joss, J. (1995). Nowcasting of motion and growth of precipitation with radar over a complex orography. *Journal of Applied Meteorology and Climatology*, *34*(6), 1286–1300. https://doi.org/10.1175/1520-0450(1995)034<1286:NOMAGO>2.0.CO;2

Long, X., Gan, C., Melo, G., Liu, X., Li, Y., Li, F., & Wen, S. (2018). Multimodal keyless attention fusion for video classification. In *Proceedings of the AAAI Conference on Artificial Intelligence* (Vol. 32, pp. 1). Retrieved from https://ojs.aaai.org/index.php/AAAI/article/view/12319

Lucas, B. D., & Kanade, T. (1981). *An iterative image registration technique with an application to stereo vision* (Vol. 81).

Matsuoka, D., Watanabe, S., Sato, K., Kawazoe, S., Yu, W., & Easterbrook, S. (2020). Application of deep learning to estimate atmospheric gravity wave parameters in reanalysis data sets. *Geophysical Research Letters*, *47*, e2020GL089436. https://doi.org/10.1029/2020GL089436

Pandeya, Y. R., & Lee, J. (2021). Deep learning-based late fusion of multimodal information for emotion classification of music video. *Multimedia Tools and Applications*, *80*(2), 2887–2905. https://doi.org/10.1007/s11042-020-08836-3

Petersik, P. J., & Dijkstra, H. A. (2020). Probabilistic forecasting of El Niño using neural network models. *Geophysical Research Letters*, *47*, e2019GL086423. https://doi.org/10.1029/2019GL086423

Reichstein, M., Camps-Valls, G., Stevens, B., Jung, M., Denzler, J., Carvalhais, N., & Prabhat (2019). Deep learning and process understanding for data-driven Earth system science. *Nature*, *566*, 195–204. https://doi.org/10.1038/s41586-019-0912-1

Romine, G. S., Burgess, D. W., & Wilhelmson, R. B. (2008). A dual-polarization-radar-based assessment of the 8 May 2003 Oklahoma City area tornadic supercell. *Monthly Weather Review*, *136*(8), 2849–2870. https://doi.org/10.1175/2008MWR2330.1

Ronneberger, O., Fischer, P., & Brox, T. (2015). U-net: Convolutional networks for biomedical image segmentation. In *International Conference on Medical Image Computing and Computer-Assisted Intervention* (pp. 234–241). Springer. https://doi.org/10.1007/978-3-319-24574-4_28

Seliga, T. A., & Bringi, V. N. (1976). Potential use of radar differential reflectivity measurements at orthogonal polarizations for measuring precipitation. *Journal of Applied Meteorology and Climatology*, *15*(1), 69–76. https://doi.org/10.1175/1520-0450(1976)015<0069:PUORDR>2.0.CO;2

Seliga, T. A., & Bringi, V. N. (1978). Differential reflectivity and differential phase shift: Applications in radar meteorology. *Radio Science*, *13*(2), 271–275. https://doi.org/10.1029/RS013i002p00271

Shi, X., Chen, Z., Wang, H., Yeung, D. Y., Wong, W. K., & Woo, W. C. (2015). *Convolutional LSTM network: A machine learning approach for precipitation nowcasting*. arXiv:1506.04214.

Shi, X., Gao, Z., Lausen, L., Wang, H., Yeung, D. Y., Wong, W. K., & Woo, W. C. (2017). *Deep learning for precipitation nowcasting: A benchmark and a new model*. arXiv:1706.03458.

Sønderby, C. K., Espeholt, L., Heek, J., Dehghani, M., Oliver, A., Salimans, T., & Kalchbrenner, N. (2020). *MetNet: A neural weather model for precipitation forecasting*. arXiv:2003.12140.

Sun, J., Xue, M., Wilson, J. W., Zawadzki, I., Ballard, S. P., Onvlee-Hooimeyer, J., et al. (2014). Use of NWP for nowcasting convective precipitation: Recent progress and challenges. *Bulletin of the American Meteorological Society*, *95*(3), 409–426. https://doi.org/10.1175/BAMS-D-11-00263.1

Thurai, M., Bringi, V. N., Szakáll, M., Mitra, S. K., Beard, K. V., & Borrmann, S. (2009). Drop shapes and axis ratio distributions: Comparison between 2D video disdrometer and wind-tunnel measurements. *Journal of Atmospheric and Oceanic Technology*, *26*(7), 1427–1432. https://doi.org/10.1175/2009jtecha1244.1

Tran, Q. K., & Song, S. K. (2019). Computer vision in precipitation nowcasting: Applying image quality assessment metrics for training deep neural networks. *Atmosphere*, *10*(5), 244. https://doi.org/10.3390/atmos10050244

Tseng, K. L., Lin, Y. L., Hsu, W., & Huang, C. Y. (2017). Joint sequence learning and cross-modality convolution for 3D biomedical segmentation. In *Proceedings of the IEEE Conference on Computer Vision and Pattern Recognition* (pp. 6393–6400). https://doi.org/10.1109/cvpr.2017.398

Veillette, M., Samsi, S., & Mattioli, C. (2020). SEVIR: A storm event imagery dataset for deep learning applications in radar and satellite meteorology. *Advances in Neural Information Processing Systems*, *33*.

Wang, M., Zhao, K., Xue, M., Zhang, G., Liu, S., Wen, L., & Chen, G. (2016). Precipitation microphysics characteristics of a Typhoon Matmo (2014) rainband after landfall over eastern China based on polarimetric radar observations. *Journal of Geophysical Research: Atmospheres*, *121*, 12415–12433. https://doi.org/10.1002/2016JD025307

Wang, Y., Long, M., Wang, J., Gao, Z., & Yu, P. S. (2017). PredRNN: Recurrent neural networks for predictive learning using spatiotemporal LSTMs. In *Proceedings of the 31st International Conference on Neural Information Processing Systems* (pp. 879–888).

Wen, J., Zhao, K., Huang, H., Zhou, B., Yang, Z., Chen, G., et al. (2017). Evolution of microphysical structure of a subtropical squall line observed by a polarimetric radar and a disdrometer during OPACC in Eastern China. *Journal of Geophysical Research: Atmospheres*, *122*, 8033–8050. https://doi.org/10.1002/2016JD026346

Weyn, J. A., Durran, D. R., & Caruana, R. (2020). Improving data-driven global weather prediction using deep convolutional neural networks on a cubed sphere. *Journal of Advances in Modeling Earth Systems*, *12*, e2020MS002109. https://doi.org/10.1029/2020MS002109

Wilson, J. W., Crook, N. A., Mueller, C. K., Sun, J., & Dixon, M. (1998). Nowcasting thunderstorms: A status report. *Bulletin of the American Meteorological Society*, *79*(10), 2079–2099. https://doi.org/10.1175/1520-0477(1998)079<2079:NTASR>2.0.CO;2

Wilson, J. W., Feng, Y., Chen, M., & Roberts, R. D. (2010). Nowcasting challenges during the Beijing Olympics: Successes, failures, and implications for future nowcasting systems. *Weather and Forecasting*, *25*(6), 1691–1714. https://doi.org/10.1175/2010WAF2222417.1

Zhao, K., Huang, H., Wang, M., Lee, W. C., Chen, G., Wen, L., et al. (2019). Recent progress in dual-polarization radar research and applications in China. *Advances in Atmospheric Sciences*, *36*(9), 961–974. https://doi.org/10.1007/s00376-019-9057-2

Zhou, K., Zheng, Y., Dong, W., & Wang, T. (2020). A deep learning network for cloud-to-ground lightning nowcasting with multisource data. *Journal of Atmospheric and Oceanic Technology*, *37*(5), 927–942. https://doi.org/10.1175/JTECH-D-19-0146.1

Zhou, T., Ruan, S., & Canu, S. (2019). A review: Deep learning for medical image segmentation using multi-modality fusion. *Array*, *3*, 100004. https://doi.org/10.1016/j.array.2019.100004

Zrnić, D. S., & Ryzhkov, A. (1996). Advantages of rain measurements using specific differential phase. *Journal of Atmospheric and Oceanic Technology*, *13*(2), 454–464. https://doi.org/10.1175/1520-0426(1996)013<0454:AORMUS>2.0.CO;2